Interface optical-phonon modes and electron–interface-phonon interactions in wurtzite GaN/AlN quantum wells

Jun-jie Shi
State Key Laboratory for Mesoscopic Physics, and School of Physics, Peking University, Beijing 100871, People's Republic of China
(Received 29 May 2003; published 23 October 2003)

Based on the dielectric-continuum model and Loudon's uniaxial crystal model, the equation of motion for the *p*-polarization field in an arbitrary wurtzite multilayer heterostructure is solved exactly for the interface optical-phonon modes. The polarization eigenvector, the dispersion relation, and the electron–interface-phonon interaction Fröhlich-like Hamiltonian are derived using the transfer-matrix method. The analytical formulas can be directly applied to single heterojunctions, single and multiple quantum wells (QW's), and superlattices. Considering the strains of QW structures and the anisotropy effects of wurtzite crystals, the dispersion relations of the interface phonons and the electron–interface-phonon coupling strengths are investigated for GaN/AlN single and coupled QW's. We find that there are four (eight) interface optical-phonon branches with definite symmetry with respect to the symmetric center of a single (coupled) QW. Typical features in the dispersion curves are evidenced which are due to the anisotropy effects of wurtzite crystals. The lower-frequency modes are much more important for the electron–interface-phonon interactions than the higher-frequency modes. For the lower-frequency interface phonons, the intensity of the electron-phonon interactions is reduced due to the strain effects of the QW structures. For the higher-frequency interface modes, the influence of the strains on the electron-phonon interactions can be ignored.

DOI: 10.1103/PhysRevB.68.165335 PACS number(s): 78.67.De, 63.20.Dj, 63.20.Kr, 63.22.+m

I. INTRODUCTION

Quantum heterostructures based on the wide-band-gap group-III nitrides GaN, AlN, InN, and their ternary compounds have recently attracted much attention due to conspicuous device applications, such as the high-brightness blue/green light emitting diodes (LED's) and laser diodes (LD's).[1–9] Besides their potential applications in electronics and optoelectronics, they are also quite attractive from a purely physical viewpoint. Their fundamental physical properties can be largely affected and even determined by the spatial quantization of the electron states, the anisotropy of the crystal structures and the strains of the heterostructures.

Group-III nitrides usually crystallize in the hexagonal wurtzite structure (space group C_{6v}^4), which is composed of two interpenetrating hexagonal close-packed sublattices, displaced along the c axis (z axis) by 5/8 of the cell height c. The primitive cell in wurtzites contains four atoms. Consequently, there are nine optical and three acoustical phonon branches for a given phonon wave vector.[10] Only two optical-phonon branches are both Raman and infrared active. They correspond to the extraordinary A_1 and E_1 phonons in irreducible representation at the Γ point.[11–15] The wurtzites are uniaxial crystals with the optical axis coinciding with the c axis of the crystal structure that is perpendicular to the hexagons. Due to the optical anisotropy of uniaxial crystals, the long-wavelength optical lattice vibrations can be classified according to mutual orientation between the c axis, the phonon wave vector $\vec{q}$, the electric field $\vec{E}$, and the polarization $\vec{P}$.[16,17] This classification divides the lattice vibrations into two groups: the ordinary and extraordinary optical phonons. The ordinary phonons with E_1 symmetry are always transverse (both $\vec{E}$ and $\vec{P}$ are perpendicular to $\vec{q}$ and the c axis simultaneously) and polarized in the $\perp$ plane for a given wave vector $\vec{q}$. The frequencies of the ordinary phonons are independent of the angle θ between the phonon wave vector $\vec{q}$ and the c axis. The extraordinary phonons are associated with z- and $\perp$-polarized vibrations. The z-polarized mode has A_1 symmetry and the $\perp$-polarized one has E_1 symmetry. When the angle θ is 0, one vibration is a A_1(LO) phonon and the other is a E_1(TO) phonon. If θ is varied from 0 to $\pi/2$, these modes gradually become a A_1(TO) and a E_1(LO) phonon, respectively, without having a proper LO or TO character and A_1 or E_1 symmetry. Therefore the phonon spectra in wurtzites are much more complicated than those in cubic crystals.[18–25] It has been known that, at room and higher temperatures, the scattering of electrons by optical phonons play a dominant role for various electronic properties. The electron-phonon interactions and scattering govern a number of important properties of quantum heterostructures, including hot-electron relaxation rates, interband transition rates, and room-temperature exciton lifetimes, etc. The optical and transport properties of wurtzite quantum heterostructures can also be strongly influenced by the electron-phonon interactions.[26–28] Hence the understanding of lattice dynamics and electron-phonon interactions in wurtzite semiconductor quantum heterostructures has been primitive, which has not only important theoretical meaning but also practical significance for device applications.

In order to investigate optical-phonon modes and electron-phonon interactions in polar semiconductor quasi-two-dimensional (Q2D) quantum heterostructures, several theoretical models have been proposed successively. The principal models are the microscopic calculation model of the phonon spectra based on first-principles interatomic force constants,[29,30] the standard dielectric-continuum (DC) model using the electrostatic boundary conditions (BC's),[18,31–33] the guided-mode model considering the hydrodynamic BC's at

the interfaces,[34] and the modified dielectric-continuum (MDC) model.[35,36] The MDC model was introduced by Huang and Zhu in Ref. 35, in which only nonorthogonal polarization eigenfunctions are derived. With the help of Schmidt's orthogonalization method, Haupt and Wendler[36] found a complete set of orthonormalized confined eigenmodes satisfying both electrostatic and mechanical BC's, i.e., the continuity of the tangential component of the electric field $\vec{E}$, the z component of the electric displacement vector $\vec{D}$, and the relative ionic displacement field $\vec{w} \sim \vec{E}$ at the heterointerfaces. The work of Haupt and Wendler[36] can thus be regarded as an improvement of the MDC model of Ref. 35. The main difference of the DC, MDC, and the guided-mode models is the choice of BC's for the polarization eigenmodes, which can be reflected in some physical problems, in which the selection rules become important. This is because the LO phonons have different symmetry in these models. However, as pointed out by Klimin *et al.*,[37] the choice of the BC's becomes less critical if the observed physical quantities include sum over all phonon modes. Moreover, the microscopic calculations of the phonon spectra[30] clearly show that both the DC and the MDC models are more reliable than the guided-mode model for the description of the phonon modes in Q2D multilayer heterostructures and the improvements of the complicated MDC model to the DC model are small in magnitude, which has also been confirmed by the numerical calculations of the electron-phonon scattering rates in a quantum well (QW) in Ref. 36. Hence the DC model has been extensively used in the recent literature due to its good agreement with the microscopic calculations of the phonon spectra[30] and the experiments[38] and its simplicity.

Based on the DC model[18] and Loudon's uniaxial crystal model,[16,17] some theoretical investigations have been devoted to the polar optical phonons in wurtzite GaN/AlN single heterojunctions, single QW's,[11,12] and infinite superlattices (SL's).[13] Electron-optical-phonon scattering in wurtzite crystals and single QW's was investigated in Refs. 14 and 15. The polaron properties of III-V nitride compounds were studied in Refs. 39–41. The polar optical phonons and their interactions with electrons in GaN/AlN quantum dots (QD's) were also treated in Refs. 42–44. The size dependence of exciton-LO-phonon coupling in $In_xGa_{1-x}N$/GaN-based QW's and QD's was also studied in Ref. 45. The lattice dynamics of group-III nitride (110) surfaces was studied using the adiabatic bond-charge model within a supercell approach in Ref. 46. Demangeot *et al.*[47] investigated resonant Raman scattering in hexagonal $Al_xGa_{1-x}N$ alloys, which confirmed the role of the Fröhlich electron-phonon interactions in the scattering processes. Phonons and free-carrier effects in wurtzite GaN/AlGaN SL's were studied by infrared spectroscopic ellipsometry and micro-Raman scattering in Ref. 48. Angular dispersion of polar phonons and Raman scattering due to extraordinary phonons in wurtzite GaN/AlN SL's were also investigated.[49,50] The experimental results of Refs. 49 and 50 were found to be in good agreement with the calculations based on the DC model, which confirmed the correctness of the DC model for the description of the lattice dynamic properties of wurtzite QW's and SL's. A microscopic theory for the generation and propagation of coherent acoustic phonons in $In_xGa_{1-x}N$/GaN multiple quantum wells (MQW's) was presented.[51] Phonon sidebands in InGaN/GaN MQW's were also investigated in Ref. 52. The LO phonon-assisted luminescence of the shallow donor-bound excitons and free excitons in the GaN films was also investigated at different temperatures.[53] By using Raman-scattering technology, Bergman *et al.*[54] investigated phonon lifetimes in wurtzite AlN and GaN; Alexson *et al.*[55] further studied the confined phonons and the phonon-mode properties of wurtzite III-V nitrides. Resonant Raman scattering on free and bound excitons in GaN was also treated.[56] However, as we know, MQW's or finite SL's rather than the single QW's or infinite SL's are adopted in the commonly used GaN-based optoelectronic devices, such as LED's and LD's.[2,6,7] Obviously, it is necessary and imperative to investigate the lattice dynamic properties of a wurtzite Q2D multilayer heterostructure due to the strong influence of electron-phonon interactions on the optical and transport properties of group-III nitride semiconductors.[26–28] Moreover, as pointed out by Zhang *et al.*,[26] the phonon modes and the electron-phonon interactions in wurtzite multilayer heterostructures are less understood. The subject of the present contribution is to solve the interface optical-phonon modes and derive the electron–interface-phonon interaction Fröhlich-like Hamiltonian in wurtzite Q2D MQW's or SL's with arbitrary layer numbers by means of the DC model and Loudon's uniaxial crystal model.

The paper is organized as follows. In Sec. II, basic equations to describe the polar optical phonons in bulk wurtzite crystals are outlined for self-sufficiency. The interface optical-phonon modes in a wurtzite Q2D multilayer heterostructure with arbitrary layer numbers are solved. Moreover, the electron–interface-phonon interaction Fröhlich-like Hamiltonian is also derived. The numerical results for the dispersion relations, the electron–interface-phonon coupling functions in GaN/AlN single and coupled QW's, are given and discussed in Sec. III. Finally, the main conclusions obtained in this paper are summarized in Sec. IV.

II. THEORY

A. Phonons in bulk wurtzite crystals

For a bulk wurtzite crystal and within the framework of the DC model, the field associated with the polar optical modes in the nonretardation limit satisfies Maxwell's equations,

$$\nabla \times \vec{E} = 0, \tag{2.1}$$

$$\nabla \cdot \vec{D} = 0, \tag{2.2}$$

with

$$\vec{D} = \varepsilon_0 \vec{E} + \vec{P} = \varepsilon_0 \epsilon(\omega) \vec{E}, \tag{2.3}$$

$$\vec{P} = \varepsilon_0 \chi(\omega) \vec{E}, \tag{2.4}$$

$$\epsilon(\omega)=1+\chi(\omega), \tag{2.5}$$

where ε_0 is the absolute dielectric constant.

Due to the anisotropy of wurtzite crystals, the polar phonon frequencies and the dielectric function become direction dependent. The dielectric tensor can be written as

$$\epsilon(\omega)=\begin{pmatrix} \epsilon_{\perp}(\omega) & 0 & 0 \\ 0 & \epsilon_{\perp}(\omega) & 0 \\ 0 & 0 & \epsilon_{z}(\omega) \end{pmatrix}, \tag{2.6}$$

where

$$\epsilon_{\perp}(\omega)=\epsilon_{\perp}^{(\infty)}\frac{\omega^2-\omega_{\perp,L}^2}{\omega^2-\omega_{\perp,T}^2} \tag{2.7}$$

for E_1 phonons and

$$\epsilon_{z}(\omega)=\epsilon_{z}^{(\infty)}\frac{\omega^2-\omega_{z,L}^2}{\omega^2-\omega_{z,T}^2} \tag{2.8}$$

for A_1 phonons. Here the subscripts $\perp$ and z denote the perpendicular direction and the parallel direction of the z axis, $\epsilon_{\perp}^{(\infty)}$ and $\epsilon_{z}^{(\infty)}$ are the optical dielectric constants, $\omega_{\perp,L}$ and $\omega_{z,L}$ are the zone center longitudinal E_1(LO) and A_1(LO) phonon frequencies, and $\omega_{\perp,T}$ and $\omega_{z,T}$ are the zone center transverse E_1(TO) and A_1(TO) phonon frequencies of the bulk materials.

We have known that there are two kinds of important optical-phonon modes in a bulk wurtzite crystal.[16,17] One is the so-called ordinary phonons. Their polarization modes are purely transverse modes (s-polarization modes). Since these modes are completely decoupled from the other vibrational modes, we will not discuss them in this paper. The other is the extraordinary phonons, for which the orientation of $\vec{E}$ and $\vec{P}$ with respect to $\vec{q}=(\vec{q}_{\perp},q_z)$ and the c axis is more complicated. The dispersion relation of the extraordinary phonons depend on the angle θ between the phonon wave vector $\vec{q}$ and the c axis and is given as[16,17]

$$\epsilon_{\perp}(\omega)\sin^2\theta+\epsilon_{z}(\omega)\cos^2\theta=0. \tag{2.9}$$

If we define

$$q_{\perp}=q\cdot\sin\theta,$$

$$q_z=q\cdot\cos\theta, \tag{2.10}$$

Eq. (2.9) can be further rewritten as

$$\epsilon_{\perp}(\omega)q_{\perp}^2+\epsilon_{z}(\omega)q_z^2=0. \tag{2.11}$$

Without loss of generality, we can assume that both $q_{\perp}$ and ω are real and positive.[11–13] In the case of $q_{\perp}\neq 0$, one can obtain from Eq. (2.11) the following important conclusions. If we let

$$\frac{\epsilon_{\perp}(\omega)}{\epsilon_{z}(\omega)}<0, \tag{2.12}$$

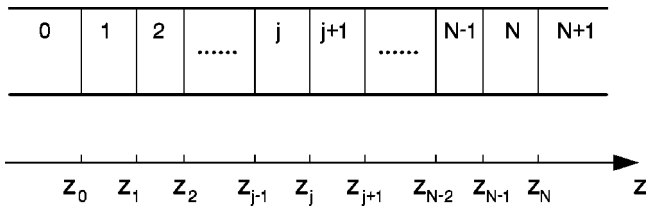

FIG. 1. A general $N+2$-layer Q2D wurtzite heterostructure. Here the z axis is taken along the [0001] direction (c axis).

q_z thus becomes purely real, which corresponds to the oscillating waves.[12] Moreover, if we let,

$$\frac{\epsilon_{\perp}(\omega)}{\epsilon_{z}(\omega)}>0, \tag{2.13}$$

q_z is purely imaginary, and the corresponding waves become the decaying ones.[12]

B. Interface optical-phonon modes in a wurtzite multilayer heterostructure

In order to investigate the optical-phonon modes and the electron-phonon interactions in wurtzite MQW's or finite SL's, let us now consider an arbitrary wurtzite Q2D multilayer heterostructure shown in Fig. 1. The heterointerfaces are located at $z=z_0,z_1,\ldots,z_{N-1}$, and z_N. Here, we take the z axis (c axis) to be perpendicular to the interfaces. In the limiting case of $q_{\perp}\rightarrow 0$, we can prove from Eq. (2.11) that the completely confined modes can exist in a wurtzite Q2D multilayer heterostructure. These phonons are strictly confined by the heterointerfaces and are highly degenerate vibrating modes with A_1(LO) phonon frequency $\omega_{z,L}^{(j)}$ in the layer j. The confined E_1(TO) phonons of the layer j (Ref. 13) will not be discussed in the present paper because the electron does not couple to TO phonons.[18] Moreover, in the case of $q_{\perp}\neq 0$, we can derive the equations for the p-polarization field $\vec{\pi}(q_{\perp},z)\equiv(P_{\perp}=P_x,P_z)$ in the layer j as follows:

$$\chi_{\perp,j}^{-1}(\omega)\frac{d}{dz}P_{\perp}^{(j)}(z)-iq_{\perp}\chi_{z,j}^{-1}(\omega)P_z^{(j)}(z)=0, \tag{2.14}$$

and

$$iq_{\perp}\frac{\epsilon_{\perp,j}(\omega)}{\chi_{\perp,j}(\omega)}P_{\perp}^{(j)}(z)+\frac{\epsilon_{z,j}(\omega)}{\chi_{z,j}(\omega)}\frac{d}{dz}P_z^{(j)}(z)=0. \tag{2.15}$$

Based on the standard DC model,[18] the solutions of Eqs. (2.14) and (2.15) should satisfy the following electrostatic BC's at the interface $z=z_j$ ($j=0,1,\ldots,N$), namely

$$\chi_{\perp,j}^{-1}(\omega)P_{\perp}^{(j)}(z)\big|_{z=z_j}=\chi_{\perp,j+1}^{-1}(\omega)P_{\perp}^{(j+1)}(z)\big|_{z=z_j} \tag{2.16}$$

for the continuity of the tangential component of the electric field $\vec{E}$, and

$$\frac{\epsilon_{z,j}(\omega)}{\chi_{z,j}(\omega)}P_z^{(j)}(z)\bigg|_{z=z_j}=\frac{\epsilon_{z,j+1}(\omega)}{\chi_{z,j+1}(\omega)}P_z^{(j+1)}(z)\bigg|_{z=z_j} \tag{2.17}$$

for the continuity of the z component of the electric displacement vector $\vec{D}$ across the $z=z_j$ interface of the Q2D multilayer heterostructure.

It is easier to solve the coupled differential Eqs. (2.14) and (2.15) by first transforming them into one differential equation. This can be done by differentiating Eq. (2.14) with respect to z once and using Eq. (2.15) to eliminate $P_z^{(j)}(z)$. We finally obtain

$$\frac{d^2}{dz^2}P_\perp^{(j)}(z)+q_{z,j}^2P_\perp^{(j)}(z)=0. \tag{2.18}$$

The general solutions of Eq. (2.18) can be written as

$$P_\perp^{(j)}(z)=i[A_j' e^{iq_{z,j}(z-z_j)}+B_j' e^{-iq_{z,j}(z-z_j)}]. \tag{2.19}$$

Based on the above analysis [please refer to Eqs. (2.11)–(2.13)], we can confirm from Eq. (2.19) that there are five distinct types of optical-phonon modes in a wurtzite Q2D multilayer heterostructure. Following Refs. 11–13, these modes can be classified as follows. (i) The interface modes with $q_{z,j}$ purely imaginary in the layer $j(j=0,1,\ldots,N+1)$. The corresponding waves cannot propagate through the structure along the z axis and the associated fields decay exponentially away from the interfaces. (ii) The propagating modes exist in the whole structure, for which $q_{z,j}$ is purely real in the layer j. (iii) The quasiconfined modes with $q_{z,j}$ purely real in the layer j, and $q_{z,j'}$ purely imaginary in the layer j' $(j'\neq j)$. The related waves display a confined behavior in the layer j. The situation is similar to that of electrons confined in a QW of finite depth. The confinement in the layer j will lead to a quantization of $q_{z,j}$. (iv) The half-space modes with both $q_{z,0}$ and $q_{z,N+1}$ purely real mainly exist in the two semi-infinite layers $(j=0,N+1)$ in the form of the oscillating waves, and (v) the exactly confined modes with $q_\perp=0$ exist in the layer j, which can be obtained from the corresponding quasiconfined modes of the layer j in the limit $\omega\to\omega_{z,L}^{(j)}$.[13] Compared with the well-studied cubic Q2D multilayer systems, such as GaAs/AlGaAs,[18–21] the optical-phonon modes in wurtzite Q2D multilayer heterostructures are much more complicated due to the anisotropy effects of wurtzite crystals. It is well known that, in cubic Q2D multilayer heterostructures, there are only three types of the p-polarized optical-phonon modes, i.e., the interface modes, the confined LO and TO modes, and the half-space modes.[18–21] Our above results clearly indicate that two new phonon modes, i.e., the propagating modes and the quasiconfined modes, together with the interface modes, the exactly confined modes, and the half-space modes, coexist in wurtzite Q2D multilayer systems. It is more interesting to note that, even in GaAs/AlGaAs SL's, the propagating modes were observed experimentally[57] when adjacent regions have small differences in dielectric properties. Consequently, the aforementioned standard classification scheme of the optical-phonon modes in cubic Q2D multilayer heterostructures is insufficient to describe the complicated optical-phonon modes in wurtzite Q2D multilayer systems, which need to be complemented suitably, as adopted by some authors in Refs. 11–13.

In the present paper, we will pay attention to the interface modes only. For simplicity, $q_{z,j}$ is substituted by $iq_{z,j}$ in the next. By using the BC's (2.16) and (2.17) at the $z=z_j$ interface, we can obtain the following matrix formula relating the successive coefficients A_{j+1}' and B_{j+1}':

$$\begin{pmatrix} A_{j+1}' \\ B_{j+1}' \end{pmatrix}=M_j\begin{pmatrix} A_j' \\ B_j' \end{pmatrix}, \quad j=0,1,\ldots,N-1, \tag{2.20}$$

where $A_0'=0$ for the interface modes, and the matrix M_j is called the transfer matrix from the layer j to the layer $j+1$ and has been defined as

$$M_j=\frac{1}{2}\begin{pmatrix} (1+\alpha_{j,j+1})\beta_{j,j+1}e^{-q_{z,j+1}d_{j+1}} & (1-\alpha_{j,j+1})\beta_{j,j+1}e^{-q_{z,j+1}d_{j+1}} \\ (1-\alpha_{j,j+1})\beta_{j,j+1}e^{q_{z,j+1}d_{j+1}} & (1+\alpha_{j,j+1})\beta_{j,j+1}e^{q_{z,j+1}d_{j+1}} \end{pmatrix}. \tag{2.21}$$

Here $d_{j+1}\equiv z_{j+1}-z_j$ is the thickness of the layer $j+1$, and $\alpha_{j,j+1}$ and $\beta_{j,j+1}$ are defined as

$$\alpha_{j,j+1}\equiv\frac{q_{z,j}\epsilon_{z,j}(\omega)}{q_{z,j+1}\epsilon_{z,j+1}(\omega)} \tag{2.22}$$

and

$$\beta_{j,j+1}\equiv\frac{\chi_{\perp,j+1}(\omega)}{\chi_{\perp,j}(\omega)}. \tag{2.23}$$

Similarly, using Eqs. (2.16) and (2.17) at the $z=z_N$ interface and letting $B_{N+1}'=0$ for the interface modes, we have

$$\begin{pmatrix} A_{N+1}' \\ 0 \end{pmatrix}=M_N\begin{pmatrix} A_N' \\ B_N' \end{pmatrix} \tag{2.24}$$

with

$$M_N=\frac{1}{2}\begin{pmatrix} (1+\alpha_{N,N+1})\beta_{N,N+1} & (1-\alpha_{N,N+1})\beta_{N,N+1} \\ (1-\alpha_{N,N+1})\beta_{N,N+1} & (1+\alpha_{N,N+1})\beta_{N,N+1} \end{pmatrix}. \tag{2.25}$$

The coefficient B_0' in the $j=0$ layer and the coefficient A_{N+1}' in the $j=N+1$ layer have the following matrix relation:

$$\begin{pmatrix} A_{N+1}' \\ 0 \end{pmatrix}=M_{tot}\begin{pmatrix} 0 \\ B_0' \end{pmatrix}, \tag{2.26}$$

where

$$M_{\rm tot}=\begin{pmatrix} M_{11} & M_{12} \\ M_{21} & M_{22} \end{pmatrix}=M_{\rm N}M_{\rm N\text{-}1}\cdots M_0. \qquad (2.27)$$

We can obtain from Eq. (2.26) the following implicit dispersion relation for the interface phonon modes in a wurtzite Q2D multilayer heterostructure:

$$M_{22}=0. \qquad (2.28)$$

This equation is the most general expression of the interface phonon dispersion relation for an arbitrary wurtzite Q2D multilayer system.

Let us now further discuss Eq. (2.28) for some special cases. First, for a single heterojunction composed of two wurtzite materials denoted as the $j=1$ and 2 layers, the dispersion equation of the interface modes can be derived from Eq. (2.28) as follows:

$$\sqrt{\epsilon_{\perp,1}(\omega)\epsilon_{z,1}(\omega)}+\sqrt{\epsilon_{\perp,2}(\omega)\epsilon_{z,2}(\omega)}=0. \qquad (2.29)$$

Furthermore, if we let $\epsilon_{\perp,j}(\omega)=\epsilon_{z,j}(\omega)(j=1,2)$, Eq. (2.29) reduces to the corresponding result of the cubic single heterojunction,[22] as it should be. Moreover, in the case of a wurtzite double heterostructure, for example, an AlN/GaN/AlN single QW, we can obtain the following dispersion relation for the interface modes from Eq. (2.28):

$$2\epsilon^{(\infty)}_{z,\rm AlN}\epsilon^{(\infty)}_{z,\rm GaN}\sqrt{\frac{\omega^2-\omega^2_{\perp,L\rm AlN}}{\omega^2-\omega^2_{\perp,T\rm AlN}}\cdot\frac{\omega^2-\omega^2_{z,L\rm AlN}}{\omega^2-\omega^2_{z,T\rm AlN}}\cdot\frac{\omega^2-\omega^2_{\perp,L\rm GaN}}{\omega^2-\omega^2_{\perp,T\rm GaN}}\cdot\frac{\omega^2-\omega^2_{z,L\rm GaN}}{\omega^2-\omega^2_{z,T\rm GaN}}}$$
$$+\left[\epsilon^{(\infty)2}_{z,\rm AlN}\frac{\omega^2-\omega^2_{\perp,L\rm AlN}}{\omega^2-\omega^2_{\perp,T\rm AlN}}\cdot\frac{\omega^2-\omega^2_{z,L\rm AlN}}{\omega^2-\omega^2_{z,T\rm AlN}}+\epsilon^{(\infty)2}_{z,\rm GaN}\frac{\omega^2-\omega^2_{\perp,L\rm GaN}}{\omega^2-\omega^2_{\perp,T\rm GaN}}\cdot\frac{\omega^2-\omega^2_{z,L\rm GaN}}{\omega^2-\omega^2_{z,T\rm GaN}}\right]\cdot\tanh(q_{z,\rm GaN}d_{\rm GaN})=0, \qquad (2.30)$$

where $d_{\rm GaN}$ is the thickness of the GaN well layer. Furthermore, we can from Eq. (2.30) derive the same dispersion relations as Eqs. (24) and (25) of Ref. 13 for the interface modes. Our numerical calculations (Figs. 2 and 3) clearly show that, for a symmetric AlN/GaN/AlN wurtzite double heterostructure (single QW), there are only four interface optical-phonon branches with definite symmetry with respect to the symmetric center of the QW structure for a given phonon wave number $q_\perp$.

For an AlN/GaN/AlN/GaN/AlN symmetric coupled QW, we can obtain from Eq. (2.28) the following dispersion relation:

$$\left[2+\left(\alpha_{01}+\frac{1}{\alpha_{01}}\right)\cdot\tanh(q_{z,\rm GaN}d_{\rm GaN})\right]^2$$
$$-\left(\alpha_{01}-\frac{1}{\alpha_{01}}\right)^2\cdot\tanh^2(q_{z,\rm GaN}d_{\rm GaN})e^{-2q_{z,\rm AlN}d_{\rm AlN}}=0, \qquad (2.31)$$

where $d_{\rm AlN}$ is the thickness of the AlN barrier layer sandwiched between the two GaN well layers with the thickness of $d_{\rm GaN}$, and α_{01} is defined as

$$\alpha_{01}\equiv\frac{q_{z,\rm AlN}\epsilon_{z,\rm AlN}(\omega)}{q_{z,\rm GaN}\epsilon_{z,\rm GaN}(\omega)}. \qquad (2.32)$$

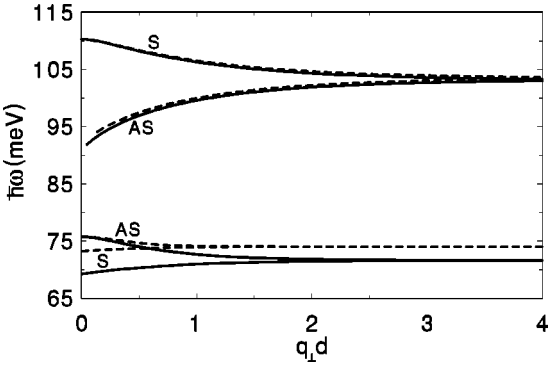

FIG. 2. Dispersion curves of the interface optical-phonon modes for a GaN QW of width $d=5$ nm sandwiched between two semi-infinite AlN barrier layers. The solid (dashed) lines are for the unstrained (strained) QW structure. The symmetric and antisymmetric modes are denoted as S and AS, respectively.

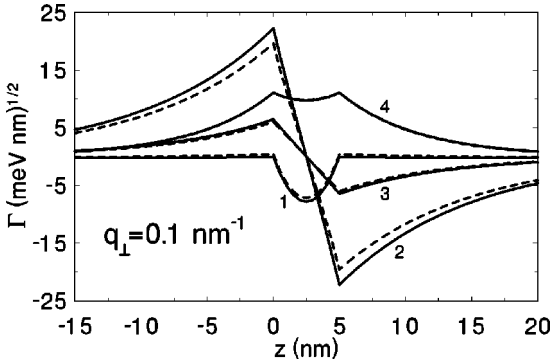

FIG. 3. Spatial dependence of the coupling function $\Gamma(q_\perp,z)$ divided by $(\hbar e^2/8A\varepsilon_0)^{1/2}$ for the interactions between an electron and interface optical phonons for the same QW as in Fig. 2 with the heterointerfaces located at $z=0$ and 5 nm, respectively. Here and in Figs. 4, 6, and 7, the numbers by the curves represent the interface phonon frequency in order of increasing magnitude. The solid and dashed lines have the same meaning as in Fig. 2.

The phonon wave numbers $q_{z,\mathrm{AlN}}$ and $q_{z,\mathrm{GaN}}$ in Eqs. (2.30), (2.31), and (2.32) are given by

$$q_{z,\mathrm{AlN}}=\sqrt{\frac{\omega^2-\omega^2_{\perp,L\mathrm{AlN}}}{\omega^2-\omega^2_{\perp,T\mathrm{AlN}}}\cdot\frac{\omega^2-\omega^2_{z,T\mathrm{AlN}}}{\omega^2-\omega^2_{z,L\mathrm{AlN}}}}\cdot q_\perp ,$$

$$q_{z,\mathrm{GaN}}=-\sqrt{\frac{\omega^2-\omega^2_{\perp,L\mathrm{GaN}}}{\omega^2-\omega^2_{\perp,T\mathrm{GaN}}}\cdot\frac{\omega^2-\omega^2_{z,T\mathrm{GaN}}}{\omega^2-\omega^2_{z,L\mathrm{GaN}}}}\cdot q_\perp . \tag{2.33}$$

In the general case, Eq. (2.31) has eight solutions with definite symmetry with respect to the symmetric center of the QW structure for a given phonon wave number $q_\perp$ (Figs. 5 and 6).

We know from Eqs. (2.20) and (2.24) that all of the other coefficients A'_j and B'_j $(j\neq 0)$ can be expressed as the coefficient B'_0 times a proportionality constant, i.e.,

$$A'_j=A_jB'_0,$$

$$B'_j=B_jB'_0. \tag{2.34}$$

The two-dimensional *p*-polarization eigenvector $\vec{\pi}(q_\perp,z)$ for the interface modes can thus be obtained from Eqs. (2.14), (2.19), and (2.34) as

$$\vec{\pi}(q_\perp,z)=B'_0\begin{cases} Q_1(q_\perp,z), & z<z_0,\\ Q_2(q_\perp,z), & z_{j-1}<z<z_j,\quad j=1,2,\ldots,N,\\ Q_3(q_\perp,z), & z>z_N,\end{cases} \tag{2.35}$$

$$Q_1(q_\perp,z)=e^{q_{z,0}(z-z_0)}[i,\gamma_0],$$

$$Q_2(q_\perp,z)=[i(A_je^{-q_{z,j}(z-z_j)}+B_je^{q_{z,j}(z-z_j)}),$$

$$\gamma_j(-A_je^{-q_{z,j}(z-z_j)}+B_je^{q_{z,j}(z-z_j)})],$$

$$Q_3(q_\perp,z)=A_{N+1}e^{-q_{z,N+1}(z-z_N)}[i,-\gamma_{N+1}].$$

In Eq. (2.35), γ_j $(j=0,1,\ldots,N+1)$ is defined as

$$\gamma_j\equiv\frac{q_{z,j}\chi_{z,j}(\omega)}{q_\perp\chi_{\perp,j}(\omega)}. \tag{2.36}$$

Considering the anisotropy effects of wurtzite crystals, we take the orthonormality condition of the two-dimensional *p*-polarization eigenvector $\vec{\pi}(q_\perp,z)$ as follows:

$$\int_{-\infty}^{\infty}dz\left(\frac{\sqrt{\eta_{\perp,j}(\omega_m)}}{\omega_{\perp,pj}}P^*_\perp(q_\perp,z),\frac{\sqrt{\eta_{z,j}(\omega_m)}}{\omega_{z,pj}}P^*_z(q_\perp,z)\right)\cdot\left(\frac{\sqrt{\eta_{\perp,j}(\omega_n)}}{\omega_{\perp,pj}}P_\perp(q_\perp,z),\frac{\sqrt{\eta_{z,j}(\omega_n)}}{\omega_{z,pj}}P_z(q_\perp,z)\right)=\delta_{mn}. \tag{2.37}$$

Here the subscripts *m* and *n* indicate the different phonon modes. Equation (2.37) can be regarded as a direct extension of the corresponding formula Eq. (29) of Ref. 18. The definitions of $\eta_j(\omega)$ and ω_{pj} are given in Ref. 22. The coefficient B'_0 in Eq. (2.35) can be obtained from Eq. (2.37) as follows:

$$B'_0=\sqrt{\frac{2}{\Lambda}}. \tag{2.38}$$

In Eq. (2.38), Λ is defined as

$$\Lambda\equiv\frac{1}{q_{z,0}}Q_{0,+}(\omega)+\frac{A^2_{N+1}}{q_{z,N+1}}Q_{N+1,+}(\omega)+\sum_{j=1}^{N}\frac{1}{q_{z,j}}\{4A_jB_jq_{z,j}d_jQ_{j,-}(\omega)-[A^2_j(1-e^{2q_{z,j}d_j})-B^2_j(1-e^{-2q_{z,j}d_j})]Q_{j,+}(\omega)\}. \tag{2.39}$$

In Eq. (2.39), $Q_{j,\pm}(\omega)$ is given by

$$Q_{j,\pm}(\omega)=\frac{\eta_{\perp,j}(\omega)}{\omega^2_{\perp,pj}}\pm\gamma^2_j\frac{\eta_{z,j}(\omega)}{\omega^2_{z,pj}}. \tag{2.40}$$

Moreover, we have the following formulas for the interface modes:[58]

$$\frac{\eta_{\perp,j}(\omega)}{\omega^2_{\perp,pj}}=\frac{[\epsilon_{\perp,j}(\omega)-\epsilon^{(\infty)}_{\perp,j}]^2}{\omega^2_{\perp,Tj}[\epsilon_{\perp,j}(\omega)-1]^2(\epsilon^{(0)}_{\perp,j}-\epsilon^{(\infty)}_{\perp,j})},$$

$$\frac{\eta_{z,j}(\omega)}{\omega^2_{z,pj}}=\frac{[\epsilon_{z,j}(\omega)-\epsilon^{(\infty)}_{z,j}]^2}{\omega^2_{z,Tj}[\epsilon_{z,j}(\omega)-1]^2(\epsilon^{(0)}_{z,j}-\epsilon^{(\infty)}_{z,j})}. \tag{2.41}$$

Here, $\epsilon^{(0)}_{\perp,j}$ and $\epsilon^{(0)}_{z,j}$ are the static dielectric constants of the layer *j*.

C. Electron-phonon-interaction in a wurtzite multilayer heterostructure

The electron-phonon interaction Fröhlich-like Hamiltonian $H_{e\text{-}ph}$ can be obtained by quantizing the energy of interaction of an electron at the position $\vec{r}$ with the scalar potential produced by the phonons, i.e., $-e\phi(\vec{r})$.[18,59] For the interface optical-phonon modes given in the above, we can obtain the electron–interface-phonon interaction Hamiltonian in an arbitrary wurtzite Q2D multilayer heterostructure as follows:[18]

$$H_{e\text{-}ph}=\sum_m\sum_{q_\perp}e^{i\vec{q}_\perp\cdot\vec{\rho}}\Gamma_m(q_\perp,z)[\hat{a}_m(\vec{q}_\perp)+\hat{a}^\dagger_m(-\vec{q}_\perp)], \tag{2.42}$$

where the electron-phonon coupling function $\Gamma_m(q_\perp,z)$, which describes the coupling strength of a single electron at the position *z* with the *m*th interface optical-phonon mode, is given as

$$\Gamma_{\mathrm{m}}(q_\perp,z)=B_0'\left(\frac{\hbar e^2}{8A\varepsilon_0\omega_{\mathrm{m}}(q_\perp)}\right)^{1/2}\begin{cases} f_1(q_\perp,z), & z<z_0, \\ f_2(q_\perp,z), & z_{\mathrm{j-1}}<z<z_{\mathrm{j}},\ \ j=1,2,\ldots,N, \\ f_3(q_\perp,z), & z>z_{\mathrm{N}}, \end{cases} \tag{2.43}$$

where A is the cross-sectional area of the heterostructure. The normal frequency $\omega_{\mathrm{m}}(q_\perp)$ of the mth branch of the interface modes can be obtained by solving the dispersion relation Eq. (2.28), and $f_{\mathrm{i}}(q_\perp,z)(i=1,2,3)$ are defined as

$$f_1(q_\perp,z)\equiv\xi_{-,0}e^{q_\perp(z-z_0)}+(\xi_{+,0}-\xi_{-,0})e^{q_{\mathrm{z},0}(z-z_0)}+\sum_{\mathrm{j}=1}^{\mathrm{N}}\left[(A_{\mathrm{j}}\xi_{+,\mathrm{j}}e^{q_{\mathrm{z,j}}d_{\mathrm{j}}}-B_{\mathrm{j}}\xi_{-,\mathrm{j}}e^{-q_{\mathrm{z,j}}d_{\mathrm{j}}})e^{q_\perp(z-z_{\mathrm{j-1}})}\right.$$
$$\left.+(B_{\mathrm{j}}\xi_{-,\mathrm{j}}-A_{\mathrm{j}}\xi_{+,\mathrm{j}})e^{q_\perp(z-z_{\mathrm{j}})}\right]+A_{\mathrm{N}+1}\xi_{+,\mathrm{N}+1}e^{q_\perp(z-z_{\mathrm{N}})}, \tag{2.44}$$

$$f_2(q_\perp,z)\equiv\xi_{+,0}e^{q_\perp(z_0-z)}+\sum_{\mathrm{l}=1}^{\mathrm{j-1}}\left[A_{\mathrm{l}}\xi_{-,\mathrm{l}}e^{q_{\mathrm{z,l}}d_{\mathrm{l}}}-B_{\mathrm{l}}\xi_{+,\mathrm{l}}e^{-q_{\mathrm{z,l}}d_{\mathrm{l}}}+(B_{\mathrm{l}}\xi_{+,\mathrm{l}}-A_{\mathrm{l}}\xi_{-,\mathrm{l}})e^{q_\perp d_{\mathrm{l}}}\right]e^{q_\perp(z_{\mathrm{l}-1}-z)}+(A_{\mathrm{j}}\xi_{-,\mathrm{j}}e^{q_{\mathrm{z,j}}d_{\mathrm{j}}}$$
$$-B_{\mathrm{j}}\xi_{+,\mathrm{j}}e^{-q_{\mathrm{z,j}}d_{\mathrm{j}}})e^{q_\perp(z_{\mathrm{j-1}}-z)}+(\xi_{+,\mathrm{j}}-\xi_{-,\mathrm{j}})(A_{\mathrm{j}}e^{q_{\mathrm{z,j}}(z_{\mathrm{j}}-z)}+B_{\mathrm{j}}e^{q_{\mathrm{z,j}}(z-z_{\mathrm{j}})})+(B_{\mathrm{j}}\xi_{-,\mathrm{j}}-A_{\mathrm{j}}\xi_{+,\mathrm{j}})e^{q_\perp(z-z_{\mathrm{j}})}$$
$$+A_{\mathrm{N}+1}\xi_{+,\mathrm{N}+1}e^{q_\perp(z-z_{\mathrm{N}})}+\sum_{\mathrm{l}=\mathrm{j}+1}^{\mathrm{N}}\left[A_{\mathrm{l}}\xi_{+,\mathrm{l}}e^{q_{\mathrm{z,l}}d_{\mathrm{l}}}-B_{\mathrm{l}}\xi_{-,\mathrm{l}}e^{-q_{\mathrm{z,l}}d_{\mathrm{l}}}+(B_{\mathrm{l}}\xi_{-,\mathrm{l}}-A_{\mathrm{l}}\xi_{+,\mathrm{l}})e^{-q_\perp d_{\mathrm{l}}}\right]e^{q_\perp(z-z_{\mathrm{l}-1})}, \tag{2.45}$$

and

$$f_3(q_\perp,z)\equiv\xi_{+,0}e^{q_\perp(z_0-z)}+\sum_{\mathrm{j}=1}^{\mathrm{N}}\left[A_{\mathrm{j}}\xi_{-,\mathrm{j}}e^{q_{\mathrm{z,j}}d_{\mathrm{j}}}-B_{\mathrm{j}}\xi_{+,\mathrm{j}}e^{-q_{\mathrm{z,j}}d_{\mathrm{j}}}+(B_{\mathrm{j}}\xi_{+,\mathrm{j}}-A_{\mathrm{j}}\xi_{-,\mathrm{j}})e^{q_\perp d_{\mathrm{j}}}\right]e^{q_\perp(z_{\mathrm{j-1}}-z)}$$
$$+A_{\mathrm{N}+1}[\xi_{+,\mathrm{N}+1}e^{q_{\mathrm{z,N}+1}(z_{\mathrm{N}}-z)}+\xi_{-,\mathrm{N}+1}(e^{q_\perp(z_{\mathrm{N}}-z)}-e^{q_{\mathrm{z,N}+1}(z_{\mathrm{N}}-z)})]. \tag{2.46}$$

In Eqs. (2.44)–(2.46), $\xi_{+,\mathrm{j}}$ and $\xi_{-,\mathrm{j}}$ $(j=0,1,\ldots,N+1)$ are given by

$$\xi_{\pm,\mathrm{j}}=\frac{1\pm\gamma_{\mathrm{j}}}{q_{\mathrm{z,j}}\pm q_\perp}. \tag{2.47}$$

The above analytical expressions (2.43)–(2.46) for the electron–interface-phonon coupling function in an arbitrary wurtzite Q2D multilayer heterostructure are universal, which can be directly applied to many important Q2D multilayer systems, such as single heterojunctions, single/multiple QW's, and SL's composed of the group-III nitrides. Moreover, our results are also useful in further investigation for the optical properties of the commonly used GaN-based devices, such as LED's and LD's.

III. NUMERICAL RESULTS AND DISCUSSION

In Sec. II, we have derived the dispersion equations and the polarization eigenvectors of the interface optical-phonon modes and the electron–interface-phonon interaction Fröhlich-like Hamiltonian in an arbitrary wurtzite Q2D multilayer heterostructure. However, the corresponding analytical formulas are quite complicated due to the anisotropy of wurtzite crystals. In order to see more clearly behaviors of the interface phonons and their interactions with electrons, as important special cases of wurtzite Q2D multilayer heterostructures, we have calculated the interface phonon dispersions and the electron–interface-phonon coupling functions for a symmetric AlN/GaN/AlN single QW and an AlN/GaN/AlN/GaN/AlN coupled QW, respectively. The parameters used in our calculations are listed in Table I. In the case of GaN and AlN, the anisotropy effect on $\varepsilon^{(\infty)}$ and $\varepsilon^{(0)}$ is weak, and we will assume that $\varepsilon_\perp^{(\infty)}=\varepsilon_{\mathrm{z}}^{(\infty)}$ (Refs. 11–13,60) and $\varepsilon_\perp^{(0)}=\varepsilon_{\mathrm{z}}^{(0)}$.[60] Considering the lattice mismatch between GaN and AlN, the thin GaN well layer experiences a biaxial compressive stress and the zone-center phonon frequencies of GaN are shifted to higher values. The magnitudes of these shifts can be estimated using the deformation potentials measured for biaxially strained wurtzite GaN as follows:[61,62]

$$\Delta\omega_\lambda=2a_\lambda\varepsilon_{\mathrm{xx}}+b_\lambda\varepsilon_{\mathrm{zz}},$$
$$\lambda=A_1(\mathrm{LO}),A_1(\mathrm{TO}),E_1(\mathrm{LO}),E_1(\mathrm{TO}). \tag{3.1}$$

Here a_λ and b_λ are the two deformation potential constants and $\varepsilon_{\mathrm{xx}}$ and $\varepsilon_{\mathrm{zz}}$ the strain elements of the GaN strained layer.

Figure 2 shows the dispersions of the interface phonons in an AlN(∞)/GaN(5 nm)/AlN(∞) symmetric single QW. We can see from Fig. 2 that there are only four interface optical-phonon solutions with definite symmetry for a given phonon wave number $q_\perp$. The modes 1 and 4 (2 and 3) (labeled from lower to higher frequency) are exactly symmetric (antisymmetric) modes with respect to the middle plane of the QW structure (Fig. 3). The dispersions of the modes 1 and 2

TABLE I. Zone-center energies (in meV) of polar optical phonons, and optical and static dielectric constants of wurtzite AlN and GaN.

Material	A_1(TO)	E_1(TO)	A_1(LO)	E_1(LO)	$\epsilon^{(\infty)}$	$\epsilon^{(0)}$
AlN [a]	75.72	83.13	110.30	113.02	4.77	8.5
GaN [a] (unstrained)	65.91	69.25	90.97	91.83	5.35	9.2
GaN (strained)	67.89 [b]	73.22 [b]	92.08 [b]	94.06		

[a]Reference 60.
[b]Reference 13.

are obvious if $q_\perp d<2$ ($d=5$ nm). A common limit value of 71.62 meV can be obtained when $q_\perp d\to\infty$. For the higher-frequency modes 3 and 4, the dispersions are evident if $q_\perp d<3$, and a common limit of 103.15 meV can also be reached in the case of $q_\perp d\to\infty$. Moreover, the influence of the strains on the dispersions of the interface phonons is evident for the two lower-frequency modes 1 and 2, and can be ignored for the higher-frequency modes 3 and 4. It is more interesting to note from Fig. 2 that a striking consequence of the anisotropy of wurtzite crystals is that the mode 3 reaches the GaN E_1(LO) phonon energy of 91.83 meV (unstrained GaN) [94.06 meV (strained GaN)] for which $q_{z,\mathrm{GaN}}=0$ and $q_\perp\neq 0$. Consequently, for very small $q_\perp$, this branch becomes the quasiconfined phonons of the GaN layer because $q_{z,\mathrm{GaN}}$ is real.

Figure 3 shows the spatial (z) dependence of the electron–interface-phonon coupling function $\Gamma(q_\perp,z)$ for the same symmetric single QW structure as in Fig. 2 ($q_\perp=0.1$ nm^{-1}). We can see from Fig. 3 that the electron interaction with the mode 1 [denoted as e-p(1)] is mainly localized in the GaN well layer, which is symmetric mode with respect to the center of the QW structure at $z=2.5$ nm; e-p(2) and e-p(3) are exact antisymmetric modes and peaks at $z=0$ or 5 nm interface; e-p(4) is symmetric mode and peak at $z=0$ or 5 nm interface. Moreover, Fig. 3 indicates that e-p(2) has the most strong electron-phonon interaction among the four interface phonon modes. Figure 3 further shows that the effects of strains due to mismatch of the lattice constants between GaN and AlN have an obvious influence on the electron-phonon interaction for the lower-frequency modes, such as, e-p(2).

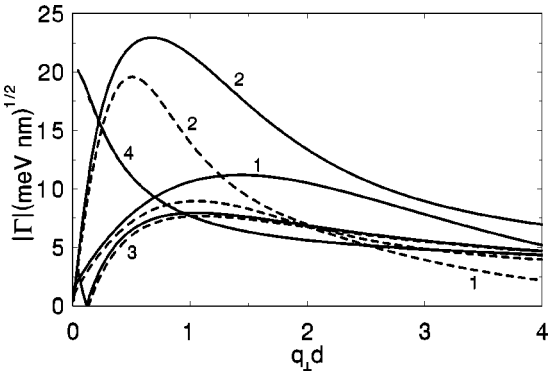

FIG. 4. Absolute values $|\Gamma(q_\perp,z)|$ divided by $(\hbar e^2/8A\varepsilon_0)^{1/2}$ as functions of $q_\perp$ for the same QW structure as in Fig. 2. The solid and dashed lines have the same meaning as in Fig. 2.

In Fig. 4, we show the absolute values $|\Gamma(q_\perp,z)|$ as functions of wave number $q_\perp$ for the same QW structure as in Fig. 2. According to Fig. 3, we have chosen $z=2.5$ nm for the mode 1, and $z=0$ nm for the modes 2, 3, and 4. Figure 4 indicates that $|\Gamma(q_\perp,z)|$ is a complicated function of $q_\perp$. The long-wavelength optical phonons are more important for the electron-phonon interactions. The e-p(2) has the most strong electron-phonon interaction. In the long-wavelength limit of $q_\perp\to 0$, e-p(2) and e-p(4) become more important. The strain effects will largely modify the electron interactions with the lower-frequency modes, such as e-p(1) and e-p(2). The strength of the electron interaction with the higher-frequency modes will basically not be affected by strains of the QW structure. Figures 3 and 4 clearly show that strains of the QW structure will reduce the strength of the electron-phonon interactions.

We further investigate the interface phonon dispersions and the electron–interface-phonon interactions in an AlN/GaN/AlN/GaN/AlN symmetric coupled QW with thickness ∞/5 nm/3 nm/5 nm/∞. The dispersion curves shown in Fig. 5 clearly indicate that, in general case, there are eight interface phonon solutions with definite symmetry for a given phonon wave number ($q_\perp d\geq 3.92$). The modes 1, 3, 6, and 8 are antisymmetric modes, and the modes 2, 4, 5, and 7 are symmetric ones with respect to the center of the QW structure at $z=6.5$ nm (Fig. 6). The dispersions of the four higher-frequency modes 5–8 are more obvious when $q_\perp d\leq 10$. A common limit of 103.15 meV can be approached if $q_\perp d\to\infty$. It is very interesting to note that the mode 5 will become the quasiconfined mode of the GaN layers for very

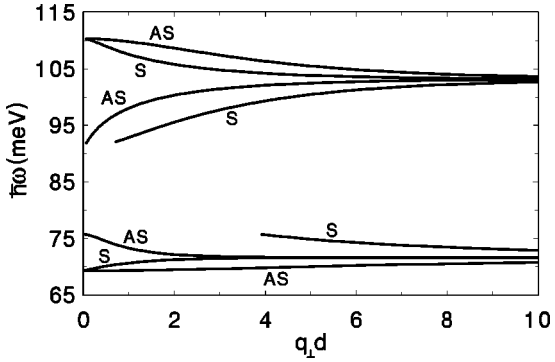

FIG. 5. Same as in Fig. 2, but for a symmetric AlN/GaN/AlN/GaN/AlN coupled QW structure with thickness ∞/5 nm/3 nm/5 nm/∞. We take $d=2d_{\mathrm{GaN}}+d_{\mathrm{AlN}}=13$ nm. Here and in Figs. 6 and 7, the calculations are performed only for unstrained QW structure.

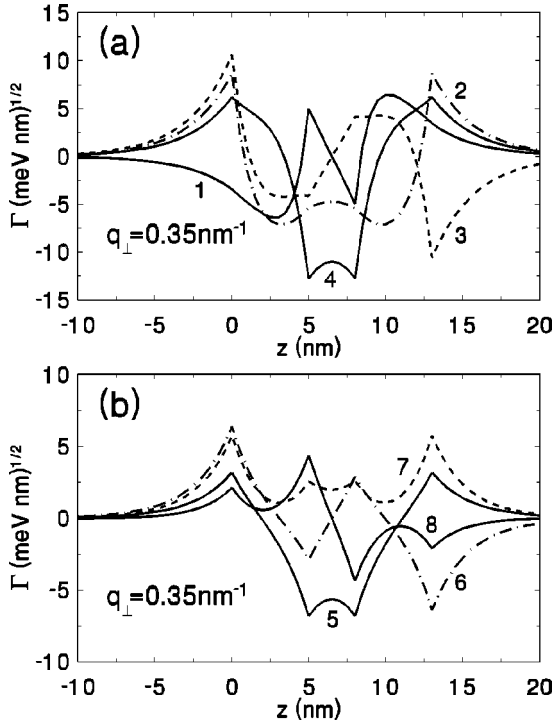

FIG. 6. Same as in Fig. 3, but for the same coupled QW structure as in Fig. 5 ($q_\perp = 0.35\ \mathrm{nm}^{-1}$) with the heterointerfaces located at $z = 0$, 5, 8, and 13 nm, respectively. Here (a) for the four lower-frequency modes 1–4, and (b) for the four higher-frequency modes 5–8.

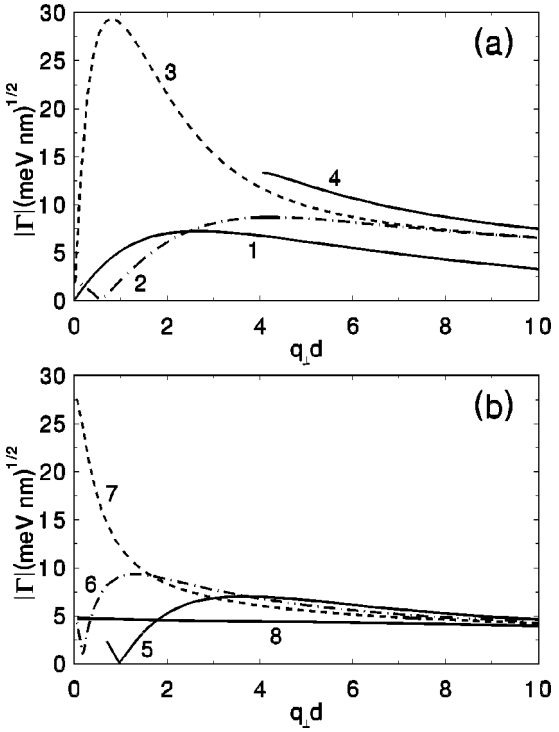

FIG. 7. Same as in Fig. 4, but for the same coupled QW structure as in Fig. 5. Here (a) for the four lower-frequency modes, and (b) for the four higher-frequency modes.

small values of $q_\perp$ ($q_\perp < 0.055\ \mathrm{nm}^{-1}$) because $q_{z,\mathrm{GaN}}$ becomes real. The physical reason has been deeply analyzed in the above (please refer to Fig. 2). Similarly, mode 4 will also become the quasiconfined mode of the AlN layers. This is because the wave number $q_{z,\mathrm{AlN}}$ becomes real due to the anisotropy effects of wurtzite crystals for a small value of $q_\perp$ ($q_\perp < 0.3\ \mathrm{nm}^{-1}$). Figure 6 shows the spatial dependence of the electron-interface-phonon coupling function $\Gamma(q_\perp, z)$ for our symmetric coupled QW with $q_\perp = 0.35\ \mathrm{nm}^{-1}$. We can see from Fig. 6 that the different modes are localized at different interfaces. The e-p(1) is antisymmetric mode and localized in the two GaN well layers; e-p(2), e-p(3), e-p(6), and e-p(7) peaks at $z = 0$ or 13 nm interface; e-p(4), e-p(5), and e-p(8) are localized at $z = 5$ or 8 nm interface. The values of $|\Gamma(q_\perp, z)|$ for the four lower-frequency modes are larger than those for the four higher-frequency modes, which is different from the case in the GaAs/AlGaAs QW's.[19–21,23–25] Moreover, Fig. 7 indicates that $|\Gamma(q_\perp, z)|$ is a complicated function of the wave number $q_\perp$. The long-wavelength optical phonons are more important for the electron-phonon interactions. The e-p(3) and e-p(7) become more important in the long-wavelength limit of $q_\perp \to 0$.

IV. CONCLUSIONS

Within the framework of the DC model and Loudon's uniaxial crystal model, we have solved the interface optical-phonon modes in a wurtzite Q2D multilayer heterostructure with arbitrary layer numbers. The *p*-polarization eigenvector, the dispersion relation, and the electron–interface-phonon interaction Fröhlich-like Hamiltonian are derived by means of the transfer-matrix method. We find from the present theory that there are five distinct types of phonon modes in a wurtzite Q2D multilayer heterostructure. The propagating modes and the quasiconfined modes, together with the interface modes, the exactly confined modes, and the half-space modes, coexist in a wurtzite Q2D multilayer heterostructure. Hence the polar optical-phonon modes in wurtzite heterostructures are much more complicated as compared with the well-studied cubic multilayer systems. However, to the best of our knowledge, it is less understood for the properties of the propagating modes and the quasiconfined modes, which need to be investigated deeply in the future.

We have further studied the dispersions of the interface optical-phonon modes and the electron-phonon coupling functions for the commonly used GaN/AlN symmetric single and coupled QW's, respectively. We find that there are four (eight) interface optical-phonon branches with definite symmetry with respect to the symmetric center of the single (coupled) QW structure for a given phonon wave number $q_\perp$. The anisotropy effects of wurtzite crystals have a large influence on the dispersion behaviors of the interface phonon modes for wurtzite QW's. The different modes are localized at the different heterointerfaces. The lower-frequency modes are much more important for the electron–interface-phonon interactions than the higher-frequency modes. The strain effects have a definite influence on the dispersions and electron-phonon interactions for the lower-frequency modes. The strength of the electron-phonon interactions will be re-

duced due to strains of the QW's. These results are important and useful for further experimental and theoretical investigations of the electron-phonon interactions and for device applications. We hope that the present work can stimulate further studies of the lattice dynamic properties, as well as device applications based on the quantum heterostructures of group-III nitrides.

ACKNOWLEDGMENTS

This work was supported by the National Natural Science Foundation of China under Grant Nos. 60276004 and 60390073, and by the Scientific Research Foundation for the Returned Overseas Chinese Scholars, State Education Ministry of China.

[1] S. Nakamura and G. Fasol, *The Blue Laser Diode* (Springer-Verlag, Berlin, 1997).
[2] B. Gil, *Group III Nitride Semiconductor Compounds* (Clarendon, Oxford, 1998).
[3] O. Ambacher, J. Phys. D **31**, 2653 (1998).
[4] S. Nakamura, Science **281**, 956 (1998).
[5] S.C. Jain, M. Willander, J. Narayan, and R.V. Overstraeten, J. Appl. Phys. **87**, 965 (2000).
[6] S. Nakamura, AAPPS Bulletin **10**, 2 (2000).
[7] S. Nakamura and S.F. Chichibu, *Introduction to Nitride Semiconductor Blue Lasers and Light Emitting Diodes* (Taylor & Francis, London, 2000).
[8] Jun-jie Shi, Solid State Commun. **124**, 341 (2002).
[9] Jun-jie Shi and Zi-zhao Gan, J. Appl. Phys. **94**, 407 (2003).
[10] C. Kittel, *Introduction to Solid State Physics* (John Wiley & Sons, New York, 1996).
[11] B.C. Lee, K.W. Kim, M.A. Stroscio, and M. Dutta, Phys. Rev. B **58**, 4860 (1998).
[12] S.M. Komirenko, K.W. Kim, M.A. Stroscio, and M. Dutta, Phys. Rev. B **59**, 5013 (1999).
[13] J. Gleize, M.A. Renucci, J. Frandon, and F. Demangeot, Phys. Rev. B **60**, 15 985 (1999).
[14] S.M. Komirenko, K.W. Kim, M.A. Stroscio, and M. Dutta, Phys. Rev. B **61**, 2034 (2000).
[15] B.C. Lee, K.W. Kim, M. Dutta, and M.A. Stroscio, Phys. Rev. B **56**, 997 (1997).
[16] R. Loudon, Adv. Phys. **13**, 423 (1964).
[17] W. Hayes and R. Loudon, *Scattering of Light by Crystals* (Wiley, New York, 1978), p. 169.
[18] L. Wendler, Phys. Status Solidi B **129**, 513 (1985).
[19] L. Wendler and R. Pechstedt, Phys. Status Solidi B **141**, 129 (1987).
[20] L. Wendler and R. Haupt, Phys. Status Solidi B **141**, 493 (1987).
[21] L. Wendler and R. Haupt, Phys. Status Solidi B **143**, 487 (1987).
[22] Jun-jie Shi, Ling-xi Shangguan, and Shao-hua Pan, Phys. Rev. B **47**, 13 471 (1993).
[23] Jun-jie Shi and Shao-hua Pan, Phys. Rev. B **51**, 17 681 (1995).
[24] Jun-jie Shi and Shao-hua Pan, J. Appl. Phys. **80**, 3863 (1996).
[25] Jun-jie Shi, B.C. Sanders, Shao-hua Pan, and E.M. Goldys, Phys. Rev. B **60**, 16 031 (1999).
[26] X.B. Zhang, T. Taliercio, S. Kolliakos, and P. Lefebvre, J. Phys.: Condens. Matter **13**, 7053 (2001).
[27] R. Zheng, T. Taguchi, and M. Matsuura, J. Appl. Phys. **87**, 2526 (2000).
[28] S.M. Komirenko, K.W. Kim, M.A. Stroscio, and M. Dutta, J. Phys.: Condens. Matter **13**, 6233 (2001).
[29] S. Baroni, P. Giannozzi, and E. Molinari, Phys. Rev. B **41**, 3870 (1990).
[30] H. Rücker, E. Molinari, and P. Lugli, Phys. Rev. B **44**, 3463 (1991); **45**, 6747 (1992).
[31] R. Fuchs and K.L. Kliewer, Phys. Rev. **140**, A2076 (1965).
[32] A.A. Lucas, E. Kartheuser, and R.G. Badro, Phys. Rev. B **2**, 2488 (1970).
[33] J.J. Licari and R. Evrard, Phys. Rev. B **15**, 2254 (1977).
[34] M. Babiker, J. Phys.: Condens. Matter **19**, 683 (1986); Physica B & C **145B**, 111 (1987); B.K. Ridley, Phys. Rev. B **39**, 5282 (1989).
[35] Kun Huang and Bangfen Zhu, Phys. Rev. B **38**, 13 377 (1988).
[36] R. Haupt and L. Wendler, Phys. Rev. B **44**, 1850 (1991).
[37] S.N. Klimin, E.P. Pokatilov, and V.M. Fomin, Phys. Status Solidi B **190**, 441 (1995).
[38] A.K. Sood, J. Menéndez, M. Cardona, and K. Ploog, Phys. Rev. Lett. **54**, 2115 (1985); R. Hessmer, A. Huber, T. Egeler, M. Haines, G. Tränkle, G. Weimann, and G. Abstreiter, Phys. Rev. B **46**, 4071 (1992).
[39] M.E. Mora-Ramos, F.J. Rodríguez, and L. Quiroga, J. Phys.: Condens. Matter **11**, 8223 (1999).
[40] M.E. Mora-Ramos, Phys. Status Solidi B **219**, R1 (2000).
[41] M.E. Mora-Ramos, Phys. Status Solidi B **223**, 843 (2001).
[42] D. Romanov, V. Mitin, and M. Stroscio, Physica B **316-317**, 359 (2002).
[43] D.A. Romanov, V.V. Mitin, and M.A. Stroscio, Phys. Rev. B **66**, 115321 (2002).
[44] D. Romanov, V. Mitin, and M. Stroscio, Physica E **12**, 491 (2002).
[45] S. Kalliakos, X.B. Zhang, T. Taliercio, P. Lefebvre, B. Gil, N. Grandjean, B. Damilano, and J. Massies, Appl. Phys. Lett. **80**, 428 (2002).
[46] H.M. Tütüncü, R. Miotto, G.P. Srivastava, and J.S. Tse, Phys. Rev. B **66**, 115304 (2002).
[47] F. Demangeot, J. Frandon, M.A. Renucci, H.S. Sands, D.N. Batchelder, O. Briot, and S. Ruffenach-Clur, Solid State Commun. **109**, 519 (1999).
[48] M. Schubert, A. Kasic, J. Šik, S. Einfeldt, D. Hommel, V. Härle, J. Off, and F. Scholz, Mater. Sci. Eng., B **82**, 178 (2001).
[49] J. Gleize, F. Demangeot, J. Frandon, M.A. Renucci, M. Kuball, B. Daudin, and N. Grandjean, Phys. Status Solidi A **183**, 157 (2001).
[50] J. Gleize, J. Frandon, F. Demangeot, M.A. Renucci, M. Kuball, J.M. Hayes, F. Widmann, and B. Daudin, Mater. Sci. Eng., B **82**, 27 (2001).
[51] G.D. Sanders, C.J. Stanton, and C.S. Kim, Phys. Rev. B **64**, 235316 (2001).
[52] R. Pecharromán-Gallego, P.R. Edwards, R.W. Martin, and I.M. Watson, Mater. Sci. Eng., B **93**, 94 (2002).
[53] S.J. Xu, W. Liu, and M.F. Li, Appl. Phys. Lett. **77**, 3376 (2000).

[54] L. Bergman, D. Alexson, P.L. Murphy, R.J. Nemanich, M. Dutta, M.A. Stroscio, C. Balkas, H. Shin, and R.F. Davis, Phys. Rev. B **59**, 12 977 (1999).
[55] D. Alexson, L. Bergman, M. Dutta, K.W. Kim, S. Komirenko, R.J. Nemanich, B.C. Lee, M.A. Stroscio, and S. Yu, Physica B **263-264**, 510 (1999).
[56] A. Kaschner, A. Hoffmann, and C. Thomsen, Phys. Rev. B **64**, 165314 (2001).
[57] D.S. Kim, A. Bouchalkha, J.M. Jacob, J.F. Zhou, J.J. Song, and J.F. Klem, Phys. Rev. Lett. **68**, 1002 (1992).
[58] Jun-jie Shi, *Electrons, Phonons, Photons, Excitons and Polarons in Low-Dimensional Semiconductor Multilayer Heterostructures* (Macquarie University, Sydney, 1999), p. 62.
[59] H. Haken, *Quantum Field Theory of Solids* (North-Holland, Amsterdam, 1976).
[60] H. Harima, J. Phys.: Condens. Matter **14**, R967 (2002).
[61] V.Y. Davydov, N.S. Averkiev, I.N. Goncharuk, D.K. Nelson, I.P. Nikitina, A.S. Polkovnikov, A.N. Smirnov, M.A. Jacobson, and O.K. Semchinova, J. Appl. Phys. **82**, 5097 (1997).
[62] F. Demangeot, J. Frandon, M.A. Renucci, O. Briot, B. Gil, and R.L. Aulombard, Solid State Commun. **100**, 207 (1996).